

Selective opposition-like control of large-scale structures in wall-bounded turbulence

J I Ibrahim¹, A Guseva² and R García-Mayoral¹

¹ Department of Engineering, University of Cambridge, Trumpington St, Cambridge CB2 1PZ, UK

² School of Aeronautics, Universidad Politécnica de Madrid, 28040 Madrid, Spain

E-mail: r.gmayoral@eng.cam.ac.uk

Abstract. We investigate the effect of controlling large-scale, logarithmic-layer turbulent structures, which have a characteristic size and aspect ratio that scale with the distance from the wall. The aim is to quantify the effect of suppressing these structures while leaving the near-wall turbulent dynamics unaltered. By affecting only the logarithmic-layer structures, it might be possible to isolate their contribution to the drag from that of the other scales in the flow. We conduct direct numerical simulations of turbulent channel flows at friction Reynolds number $Re_\tau \approx 500$ – 1000 and artificially remove certain streamwise and spanwise wavelengths of the wall-normal velocity across a range of heights. The wavelengths chosen depend on the target height (and size) of the structures that we wish to target. When these wavelengths are removed, we observe a positive, outward shift of the mean velocity profile above the target height, due to a local reduction in Reynolds shear stress, and a subsequent increase in viscous stress. Our preliminary results suggest that this shift in the mean velocity profile scales in outer units.

1. Introduction

The control of wall-bounded turbulent flows, which are prevalent in many engineering applications, has been the subject of a great deal of research over the past few decades. Strategies to reduce skin-friction drag have been of particular interest, motivated, for instance, by the fact that the skin-friction drag of a typical airliner can account for up to 50% of the total drag of the aircraft [1]. This provides significant potential for improvements in efficiency and reductions in emissions. To date, the focus has been predominantly on techniques that aim to control the near-wall turbulence cycle, due to its key role in the generation of turbulent skin friction [2, 3, 4, 5]. One such technique is the use of surface texturing [6]. In this case, so long as the direct effect of the texture is confined to the near-wall region, the only effect farther from the wall is a constant shift ΔU^+ in the mean velocity profile [7]. Other examples of near-wall control techniques include opposition control [8] and spanwise wall oscillation [9]. The near-wall region is typically defined as $y^+ \lesssim 50$, where y is the wall-normal coordinate and the ‘+’ superscript denotes scaling in wall units, i.e. normalisation by the friction velocity $u_\tau = \sqrt{\tau_w/\rho}$ and the kinematic viscosity ν , where τ_w is the wall shear stress and ρ is the density. The size of this region, in outer units, diminishes with increasing Reynolds number. It can, therefore, be shown that the drag reduction, DR , generated by techniques that target the near-wall region decreases logarithmically with increasing friction Reynolds number, Re_τ [1, 6]. In terms of ΔU^+ , the drag



reduction would be given by

$$DR = 1 - \left(\frac{1}{1 + \Delta U^+ / U_{\delta,0}^+} \right)^2, \quad (1)$$

where $U_{\delta,0}^+$ is the free stream velocity of the uncontrolled reference case. Since $U_{\delta,0}^+$ depends on the Reynolds number, it is clear from (1) that so too will the drag, even if ΔU^+ is fixed. As a result, near-wall flow-control strategies that show promise at the modest Reynolds numbers of experiments and direct simulations can be considerably less effective at the high Reynolds numbers of applications.

This has led to a growing research interest in control techniques that manipulate the larger scales of the flow, whose characteristic size scales with, say, the boundary layer thickness, δ , rather than in wall units. For example, by introducing large-scale, spanwise-varying roughness to the wall of a turbulent boundary layer, large-scale changes in the boundary layer thickness can be observed, as well as δ -scale secondary swirling motions [10, 11]. It has also been shown experimentally that it is possible to reduce the skin-friction drag in a boundary layer by targeting the large-scale motions in the logarithmic region with wall-normal jets that originate from the wall [12], although this strategy is particularly intrusive to the flow. Since the size of these kinds of structures, in outer units, does not change as the Reynolds number increases, it might be possible to produce a change in the drag that is independent of the Reynolds number.

In this paper, we investigate the role that large-scale, logarithmic-layer turbulent structures play in the generation of skin-friction drag. The focus will be on self-similar, attached structures whose streamwise and spanwise wavelengths are known to scale in outer units and have a characteristic aspect ratio that remains roughly constant within the logarithmic region of the flow [13, 14]. In the present study, we focus on channel flows, for which we define the logarithmic region approximately as $80\nu/u_\tau \lesssim y \lesssim 0.3\delta$ [15]. As discussed by Jiménez [14], at Reynolds numbers of industrial relevance, $Re_\tau \gtrsim 10^4$, a significant proportion of the turbulent dissipation takes place in the logarithmic region of the flow, which could make controlling it worthwhile. One option is to control these structures with a technique akin to opposition control [8], in which the larger wall-normal fluctuations in the logarithmic region are opposed with blowing and suction at the wall [16]. However, while this might achieve the desired effect far from the wall, the near-wall turbulent cycle could be significantly disrupted, if not eradicated entirely. In this study, the aim is to decouple these two effects and to assess the control of the logarithmic-layer structures and their dynamics alone, without directly affecting the turbulence in the near-wall region. We do this by artificially removing only the relevant wavelengths from the logarithmic region of the flow. By affecting only the logarithmic-layer structures, it might be possible to isolate their contribution to the drag from that of the other scales in the flow, hopefully gaining a better understanding of the maximum drag reduction that such control strategies could achieve. A recent study by de Giovanetti et al. [17] investigated the effect of controlling large-scale attached structures, and concluded that, at sufficiently large Reynolds numbers, most of the skin friction is generated by turbulent motions in the logarithmic region of the flow. Their method involved damping all turbulent fluctuations larger than a given spanwise wavelength across the full extent of the channel by restricting the spanwise extent of the domain, without discriminating between velocity components or particular wall-normal locations. When all spanwise wavelengths larger than 0.2δ are removed, they observed a reduction in skin friction of approximately 60%. However, since their simulations were conducted at constant mass flow rate, this could be attributed, at least in part, to the additional gain in mean velocity in the logarithmic region and above, and the subsequent drop in pressure gradient, similar to the effect seen in the minimal channel flows in [18] and [19]. In this paper, however, we remove only specific streamwise and spanwise scales from the wall-normal velocity at a range of heights within the logarithmic layer, in an attempt

to target only specific structures, while affecting the rest of the flow as little as possible.

The paper is organised as follows. First, we outline the numerical method and the series of simulations we conduct in Section 2. We then present and discuss our results in Section 3, and summarise our conclusions in Section 4.

2. Numerical method

2.1. Direct numerical simulation setup

We conduct direct numerical simulations (DNSs) of turbulent channel flows in a doubly-periodic box in the wall-parallel directions, using a code adapted from [20] and [21]. We solve the non-dimensional, unsteady, incompressible Navier–Stokes equations

$$\frac{\partial \mathbf{u}}{\partial t} + \mathbf{u} \cdot \nabla \mathbf{u} = -\nabla p + \frac{1}{Re} \nabla^2 \mathbf{u}, \quad (2)$$

$$\nabla \cdot \mathbf{u} = 0, \quad (3)$$

where $\mathbf{u} = (u, v, w)$ is the velocity vector with components in the streamwise, x , wall-normal, y , and spanwise, z , directions, respectively, p is the pressure and Re is the channel bulk Reynolds number. In the streamwise and spanwise directions, due to the periodicity of the domain, the variables are solved in Fourier space, applying the 2/3 dealiasing rule when computing the nonlinear advective terms. The wall-normal domain is discretised using a second-order centred finite difference scheme on a staggered grid. Time integration is carried out using the fractional step method [22], along with a three-step Runge-Kutta scheme. The Runge-Kutta coefficients are the same as in [23]. Semi-implicit and explicit schemes are used to approximate the viscous and advective terms, respectively.

Our simulations are conducted at two friction Reynolds numbers, $Re_\tau = \delta^+ = 550$ and 950, where δ is the channel half-height. In each case, the mean pressure gradient is fixed, which prescribes the friction velocity u_τ . Therefore, changes in drag compared to the uncontrolled reference channel are observed through changes in the channel bulk velocity, U_b , and not the friction at the wall. The viscous length scale, therefore, also remains constant. In all cases the channel half-height is $\delta = 1$, and the domain size is given by $(L_x \times L_y \times L_z)/\delta = 2\pi \times 2 \times \pi$, where L_x , L_y and L_z are the dimensions of the domain in each respective coordinate direction. This box size is sufficiently large to capture the key turbulence processes and length scales of the near-wall and logarithmic regions of the flow [24]. The grid-resolution in the wall-parallel directions is chosen such that, in dealiasing space, $\Delta x^+ \approx 9$ and $\Delta z^+ \approx 4$ for simulations at both Reynolds numbers. In the wall-normal direction, the grid is stretched such that $\Delta y_{min}^+ \approx 0.32$ and $\Delta y_{max}^+ \approx 3.0$ for $Re_\tau = 550$, and $\Delta y_{min}^+ \approx 0.35$ and $\Delta y_{max}^+ \approx 5.0$ for $Re_\tau = 950$.

2.2. Artificially removing length scales from the wall-normal velocity

The aim is to inhibit the self-similar logarithmic-layer structures discussed in Section 1, and ultimately determine their contribution to the drag. These structures may be viewed as attached vortex clusters, consisting of a sweep and an ejection, with a corresponding pair of high- and low-speed streaks [13, 14]. The typical aspect ratio of these clusters is approximately 6:2:3 in the streamwise, wall-normal and spanwise directions, respectively. That is, if the cluster is centred at y_c , then it will have a length of approximately $6y_c$ in the streamwise direction, a height of $2y_c$ in the wall-normal direction and a width of $3y_c$ in the spanwise direction. We aim to disrupt the interaction between these sweeps, ejections and streaks. We do this by removing from the flow the dominant length scales of the wall-normal velocity at the nominal mid-height of the vortex cluster, which we refer to as the target height y_t .

The wall-normal velocity in Fourier space may be written as $\hat{v}(k_x, k_z, y)$, where k_x and k_z are the streamwise and spanwise wavenumbers, respectively. The wavenumbers satisfy

Table 1. Summary of simulations conducted in this study. The target height, y_t^+ , is the nominal centre of gravity of the vortex cluster we wish to target, $\lambda_{x,t}$ and $\lambda_{z,t}$ are the target wavelengths of the wall-normal velocity that we remove from the flow, and y_f^+ is the wall-normal height, or heights, at which these wavelengths are removed. $\Delta U^+(y^+) = U^+ - U_s^+$ is the difference between the controlled and uncontrolled mean velocity profiles, $U^+(y^+)$ and $U_s^+(y^+)$, respectively. The given value of ΔU^+ is measured at $y^+ = 300$. U_δ is the mean channel centreline velocity of each case.

| Case | Line style | Re_τ | y_t^+ | $\lambda_{x,t}/y_t$ | $\lambda_{z,t}/y_t$ | y_f^+ | ΔU^+ | $\Delta U/U_\delta$ |
|------|------------|-----------|---------|---------------------|---------------------|---------|--------------|---------------------|
| 1 | — | 550 | 150 | | | 100 | 0.40 | 0.019 |
| 2 | --- | 550 | 150 | | | 0–100 | 0.76 | 0.035 |
| 3 | — · — | 550 | 150 | 2–6 | 1–3 | 150 | 0.15 | 0.007 |
| 4 | ····· | 550 | 150 | | | 0–150 | 0.64 | 0.030 |
| 5 | — | 950 | 150 | | | 100 | 0.33 | 0.014 |
| 6 | --- | 950 | 259 | 2–6 | 1–3 | 173 | 0.42 | 0.018 |
| 7 | — · — | 950 | 259 | | | 100–173 | 0.54 | 0.023 |

$-N_x/2 \leq k_x \leq N_x/2 - 1$ and $-N_z/2 \leq k_z \leq N_z/2 - 1$, where N_x and N_z are the total number of modes in each direction. Each unique pair of wavenumbers (k_x, k_z) is referred to as a ‘mode’, and the length scale of a mode is given by the pair of wavelengths associated with its wavenumbers, $(\lambda_x, \lambda_z) = (L_x/|k_x|, L_z/|k_z|)$. As a direct consequence of this definition, note that each unique pair of wavelengths (λ_x, λ_z) has contributions from four pairs of wavenumbers, i.e. the four modes $(\pm k_x, \pm k_z)$. In each case, a certain range of length scales of v will be removed from the flow, which we call the target wavelengths in the streamwise and spanwise directions, $\lambda_{x,t}$ and $\lambda_{z,t}$. This is achieved by explicitly setting to zero the relevant modes in our DNSs at every time step. We do this either at one wall-normal plane or across a range of wall-normal heights. The height, or heights, at which the wavelengths are removed is denoted by y_f , which we also refer to as the forcing height. In all cases, the range of wavelengths of v removed from the flow in the streamwise and spanwise direction is $2 \leq \lambda_{x,t}/y_t \leq 6$ and $1 \leq \lambda_{z,t}/y_t \leq 3$, which respects the aspect ratio of the vortex clusters we aim to control.

A summary of the simulations conducted in this study is provided in table 1. Note that in all cases except for case 5, in terms of the channel half-height, the target wavelengths are $0.55 \leq \lambda_{x,t}/\delta \leq 1.64$ and $0.27 \leq \lambda_{z,t}/\delta \leq 0.82$. For case 5, we have $0.32 \leq \lambda_{x,t}/\delta \leq 0.95$ and $0.16 \leq \lambda_{z,t}/\delta \leq 0.47$. The forcing heights chosen in each case should be considered exploratory at this stage. Cases 1–4, for instance, have the same nominal target height, y_t^+ , but different forcing heights, y_f^+ . Since the self-similar structures we aim to control are attached to the wall, we would expect that removing the target wavelengths from any height between the wall and the target height would, to some extent, disrupt their dynamics. Forcing at just one plane (e.g. case 1) or at every height from the wall to that plane (e.g. case 2) might provide some further insight into the effectiveness of this control strategy. The initial conditions for the forced simulations were taken from reference unforced flows at the same Reynolds number. Since the forcing is only imposed in some y planes, with no smoothing, abrupt gradients could be observed in the flow in the first instance, especially in the wall-normal velocity at the interface between forced and unforced heights. These sharp gradients were, however, observed to smooth out after the initial transient, as continuity resulted in only small values of v in the unforced plains adjacent to the forced ones. From the point of view of the forced modes, these interfaces act thereafter as impermeable-but-slipping boundaries.

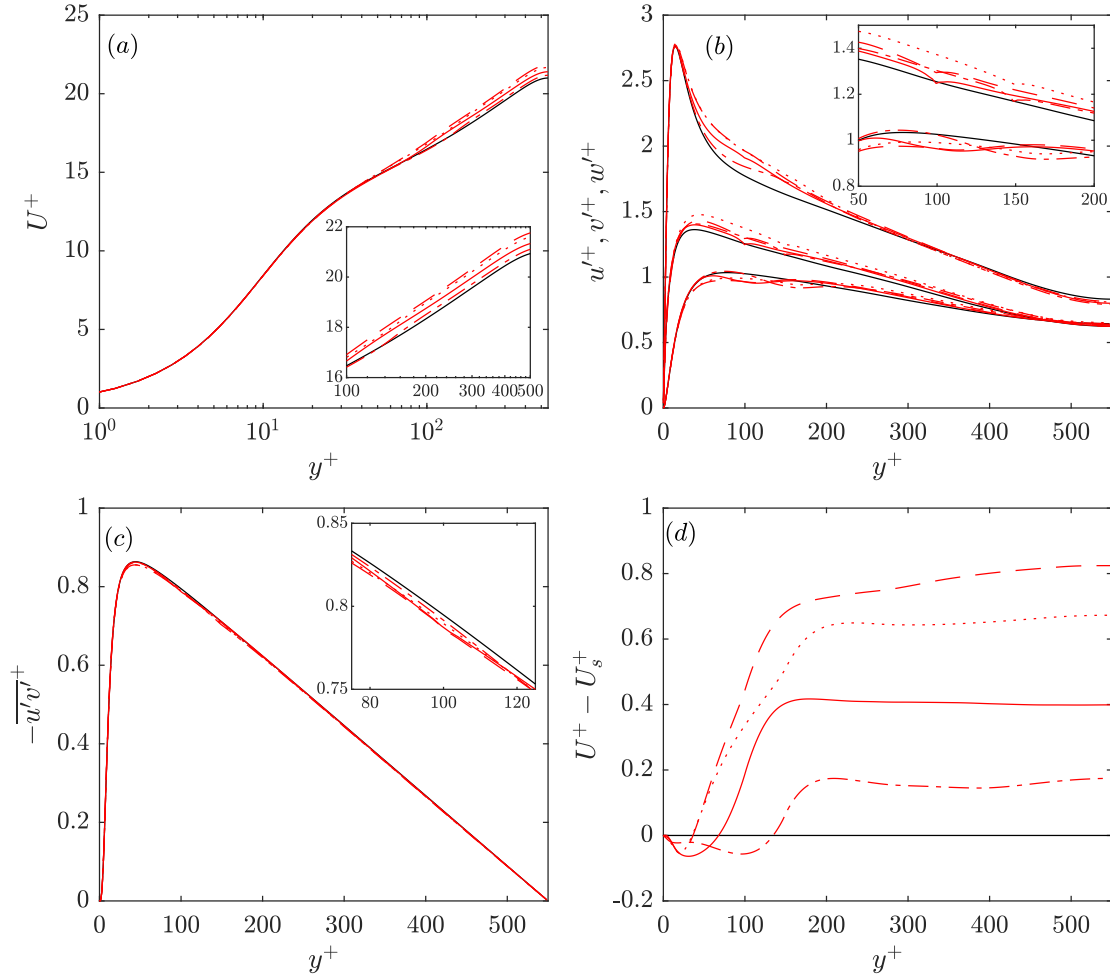


Figure 1. Statistics for cases at $Re_\tau = 550$, including $\Delta U^+(y^+) = U^+ - U_s^+$. Black lines, uncontrolled case; red lines, controlled cases. See table 1 for line styles.

3. Results and discussion

In this section, we present and discuss the results of our simulations, starting first with the four cases at $Re_\tau = 550$. The same modes are removed from the wall-normal velocity in all four simulations, with the aim of targeting the self-similar attached vortex clusters whose centre of gravity is at $y^+ \approx 150$ (see Section 2.2). However, the range of wall-normal locations over which the modes are removed is different, as shown in table 1. In two cases modes are removed at only one height, while in the other two they are removed from the wall up to a given height in the logarithmic region. Mean statistics for these cases are shown in figure 1. The effect of the control on the mean velocity profiles (figure 1a) appears to be an increase in velocity above the height at which the modes are removed, while the near-wall region and buffer layer remain unaffected, even when the modes are removed all the way down to the wall, i.e. cases 2 and 4. Notably, while there are local changes in the r.m.s. velocity fluctuations and Reynolds shear stress in the vicinity of the target height (figure 1b,c), these changes are small, particularly for $-\overline{u'v'}$. Further, in the near-wall region and far enough above the target height, the turbulent fluctuations and Reynolds shear stress essentially collapse to the uncontrolled reference data.

In Section 1, we discussed the shift ΔU^+ produced by certain near-wall control techniques,

and noted that it was constant everywhere above the near-wall region. From figure 1(a), the outward shift in the mean velocity profile generated by the removal of v modes in the logarithmic region eventually appears to become essentially constant with y^+ , far enough above the target height. We quantify this shift in terms of the difference $\Delta U^+(y^+) = U^+ - U_s^+$, where $U^+(y^+)$ and $U_s^+(y^+)$ are the controlled and uncontrolled mean velocity profiles, respectively. An approximate value for ΔU^+ , measured at $y^+ = 300$, is also given in table 1. Figure 1(d) compares the variation of ΔU^+ with y^+ for each case, and shows that in all cases, ΔU^+ is essentially constant far enough above the target height and into the outer region of the flow. This, combined with the fact that the turbulent fluctuations and Reynolds shear stress in these regions are essentially unmodified by the control, suggests that the only effect of the control far enough above the target height is this additional mean velocity, while the dynamics of turbulence remains essentially the same as in the uncontrolled case. However, at $Re_\tau = 550$, the logarithmic region of the flow is $80 \lesssim y^+ \lesssim 160$, and so is relatively thin in wall units. Therefore, there is only a very modest separation of scales between the near-wall cycle and the largest self-similar attached structures in the logarithmic region. Later, we will show results for simulations at $Re_\tau = 950$ where the logarithmic layer is somewhat larger in wall units, in order to verify whether the same shift ΔU^+ can be observed at higher Reynolds numbers. If this is indeed the case, since the size of the structures we wish to control scale with their wall-normal location, we also would expect that the effect of the control would scale in outer units.

The reason the flow near the wall is unchanged will now be discussed in more detail. The premultiplied energy spectra at $y^+ = 15$ are portrayed in figure 2 for cases 1 and 2. The figure shows that when modes are removed only at $y^+ = 100$, then there is essentially no change in the distribution of energy among length scales near the wall, compared to the uncontrolled flow. This can also be observed, qualitatively, by comparing snapshots of wall-normal velocity near the wall for the uncontrolled flow and case 1, as shown in figure 3(a,b). For case 2, however, where the modes are removed at every height from the wall up to $y^+ = 100$, we see a more noticeable change in the distribution of energy in the spectra, since the removed modes contain some energy near the wall. However, the overall effect on the near-wall dynamics is small, as confirmed by the fact that the mean velocity profile, r.m.s. fluctuations and Reynolds shear stress are essentially unmodified near the wall, as shown in figure 1. We again see no qualitative change in the snapshot of wall-normal velocity at $y^+ = 15$ for case 2 (figure 3c). The reason for this is that, while the removed v length scales are the most energetic within the logarithmic region, they contain comparatively little energy near the wall (figure 2b). The above behaviour can also be observed when comparing cases 3 and 4, although their near-wall spectra and snapshots are not shown here.

Concentrating now on the target height, $y^+ \approx 150$, the distribution of energy among length scales is essentially the same for cases 1 and 2, even though the forcing range is different, as shown in figure 4(a-d). This can be explained by the fact that, from the point of view of the forced modes, there is an impermeable, slipping wall at $y^+ \approx 100$ in both cases, even though the mean slip velocity they perceive is different in each case (figure 1d). Except for this difference in mean velocity, we would expect the effect on the turbulent fluctuations above this height to be similar in both cases. This is supported by the similar variation of ΔU^+ with y^+ for cases 1 and 2 above $y^+ = 100$ in figure 1(d). For cases 3 and 4, the distribution of energy among length scales is also essentially the same at the target height, as can be seen from figure 4(e-h), with the impermeable, slipping wall perceived by the forced modes located at $y^+ \approx 150$.

Figure 4 also demonstrates the effect of the forcing on the nonlinear scale interaction in (k_x, k_z) space that arises due to the advective terms of the Navier–Stokes equations (2). For example, while we observe only a small change in the magnitude of the Reynolds shear stress (figure 1c), it is now redistributed to larger wavelengths at the target height, as shown in figure 4(d,h). The spectra of u^2 and w^2 also exhibit changes in the distribution of energy among length scales

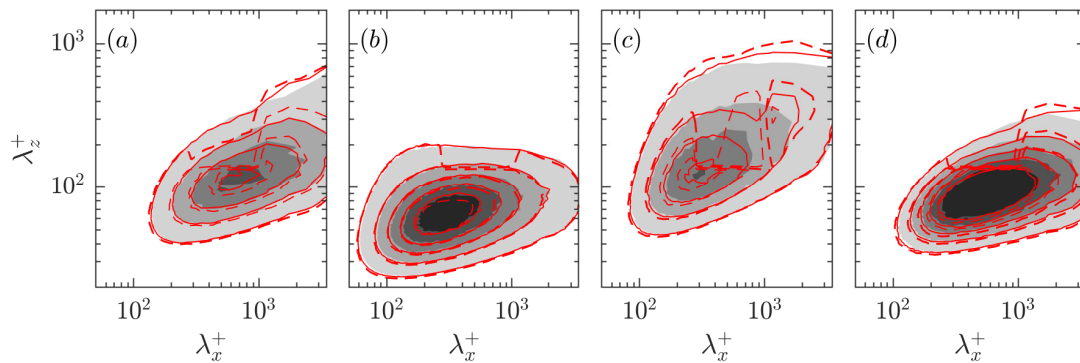


Figure 2. Premultiplied two-dimensional spectral densities of u^2 , v^2 , w^2 and uv at $y^+ = 15$ for cases 1 and 2 (red lines) compared to uncontrolled case at the same height (filled contours). See table 1 for line styles.

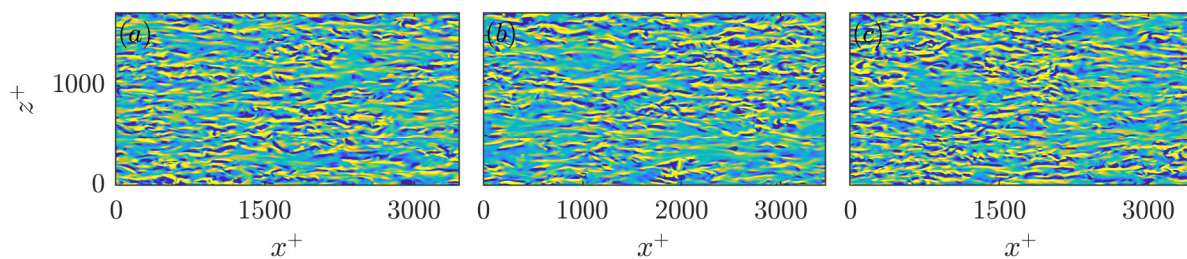


Figure 3. Instantaneous snapshots of v^+ at $y^+ = 15$ for uncontrolled case (a), case 1 (b) and case 2 (c). Blue to yellow corresponds to $v^+ = [-0.75, 0.75]$.

compared to the uncontrolled flow, even though the forcing only removes energy directly from wavelengths of v^2 . Setting certain modes of v to zero has a direct effect on other wavelengths, and not just of v but also of u and w , due to terms such as $v \partial u / \partial x$ being a convolution in (k_x, k_z) space. Eventually, this results in a wide-spectrum modification to all velocity components of the flow.

Using case 1 as an example, we now discuss why removing modes from just one plane within the logarithmic region generates an outward shift in the mean velocity profile, without affecting the turbulence farther from the wall. To do this we compare the contributions of the viscous and Reynolds shear stress to the total stress curve, which must still remain linear, in case 1 with that of the uncontrolled flow. This is given in figure 5(b). The figure shows that there is a small deficit in Reynolds shear stress in the vicinity of the forcing height, caused directly by the removal of energy from v . This is then balanced by a local increase in viscous stress, which explains why there is a sudden increase in the mean velocity around $y^+ = 100$ (figure 5a). Above the forcing height, the viscous and Reynolds stress recover to uncontrolled values, and so the shape of the mean velocity profile, i.e. dU/dy , returns to that of the uncontrolled case. This strongly suggests that the control does indeed produce a shift ΔU^+ . This is further supported by the fact that, as y^+ is increased above the target height, the premultiplied energy spectra eventually exhibit the same distribution of energy among length scales as the uncontrolled case, as shown in figure 6. This indicates that turbulence is essentially unchanged and the flow merely experiences an additional mean velocity, suggesting that turbulence far enough from the wall

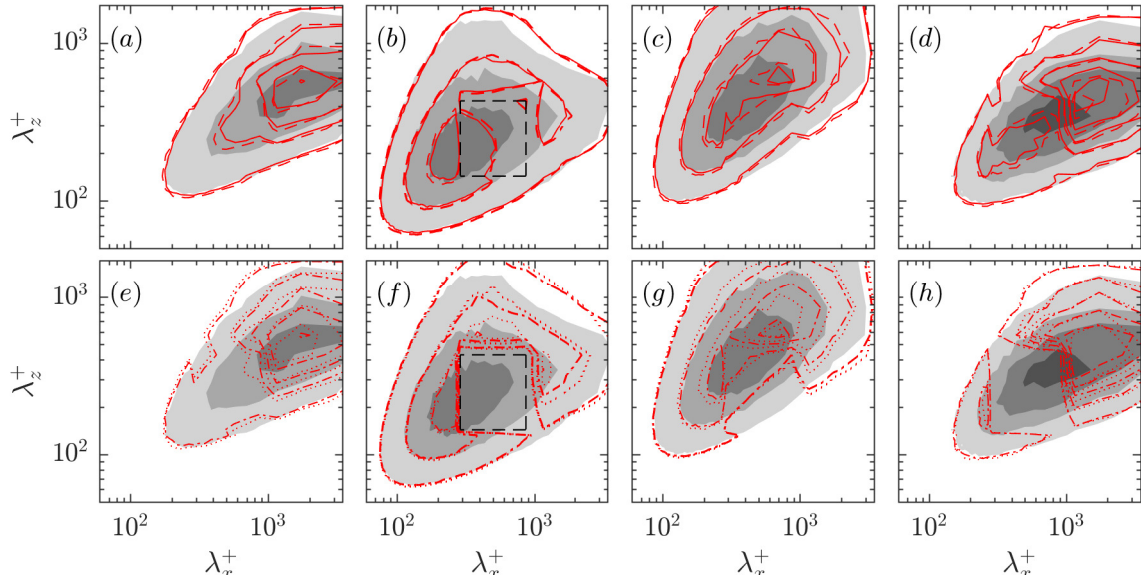


Figure 4. Premultiplied two-dimensional spectral densities of u^2 , v^2 , w^2 and uv plotted at $y^+ = 150$ for (a–d) cases 1 and 2 and (e–h) cases 3 and 4, and compared to the uncontrolled case at the same height. Filled contours, uncontrolled case; red lines, controlled cases. See table 1 for line styles. The black dashed line encloses the wavelengths of v that are removed from the flow in the forcing region, y_f^+ .

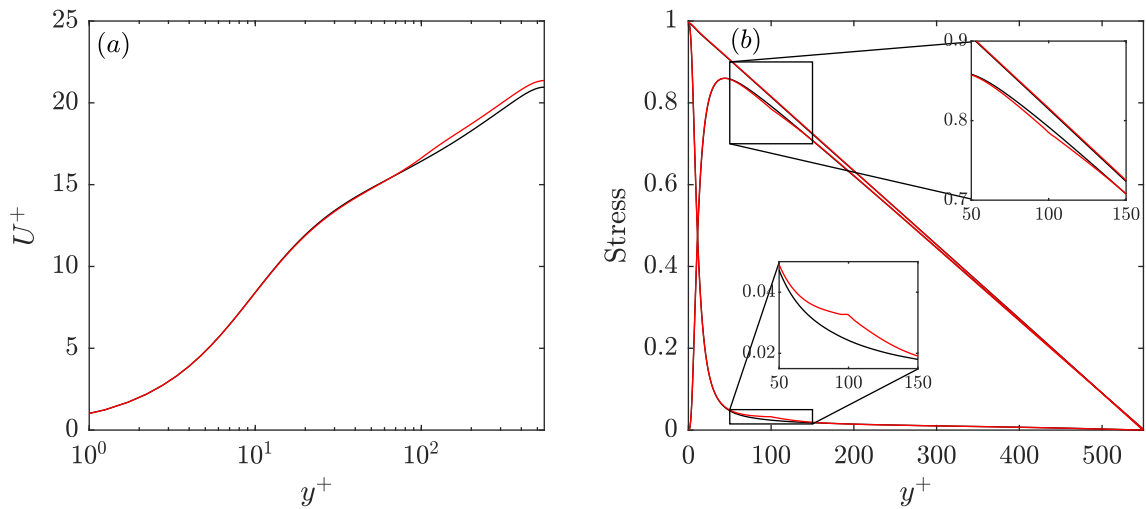


Figure 5. Additional statistics for case 1: (a) mean velocity profile for case 1 (red line) compared to uncontrolled case (black line); (b) total stress, viscous stress and Reynolds stress for case 1 (red lines) and uncontrolled case (black lines).

recovers outer-layer similarity [25].

Finally, let us present and discuss the results of our simulations conducted at $Re_\tau = 950$. There are three cases at this Reynolds number, cases 5–7, as shown in table 1. Taking as reference case 1 at $Re_\tau = 550$, case 5 is designed to be consistent in wall units, and case 6

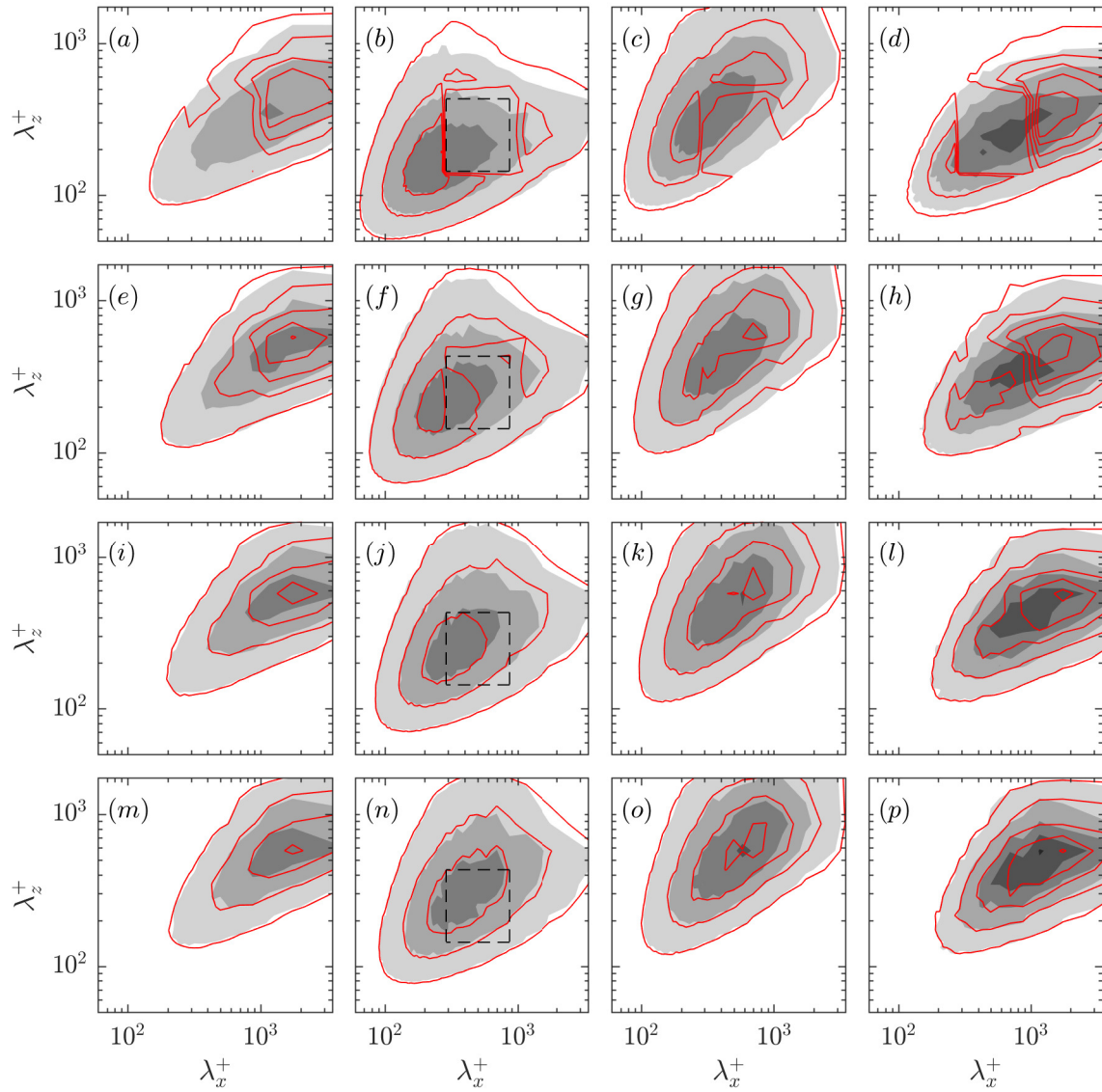


Figure 6. Premultiplied two-dimensional spectral densities of u^2 , v^2 , w^2 and uv for case 1 (red lines) compared to the uncontrolled case (filled contours) at (a–d) $y^+ = 100$, (e–h) $y^+ = 150$, (i–l) $y^+ = 200$, (m–p) $y^+ = 250$. The black dashed line encloses the wavelengths of v that are removed from the flow in the forcing region, y_f^+ .

to be consistent in outer units. The idea is to determine whether the effect of the control scales in wall or outer units. Statistics for cases 5–7 are shown in figure 7. In each case, time-averaged statistics have been collected over approximately 40 eddy turnover times. While this is sufficient to provide a good representation of the mean velocity profile, r.m.s. fluctuations and Reynolds shear stress, ΔU^+ is small and therefore requires very long sampling times, of order 100 turnover times, to provide an accurate measurement, particularly in the outer region of the flow. Therefore, our conclusions regarding ΔU^+ should be considered tentative. In figure 7, we observe very similar behaviour to all of the cases at $Re_\tau = 550$, with an increase in the mean velocity profile above the forcing region, but the flow in the near-wall region remains essentially unaffected. From figure 7(a), it would appear that the shift in the mean velocity does become essentially constant, far enough above the forcing height, consistent with the simulations at the lower Reynolds number. This is further supported by the local deficit in Reynolds shear stress at $y^+ \approx 100$ for case 5, which recovers to uncontrolled values above this height (see inset, figure 7c). We would therefore expect ΔU^+ to be essentially constant above the logarithmic region in our simulations, however the lack of sufficient sampling time is clear from figure 7(d). In table 1, as well as including an approximate value for ΔU^+ measured at $y^+ = 300$, we also include $\Delta U/U_\delta$, where U_δ is the channel centreline velocity. $\Delta U/U_\delta$ provides a measure for the effect of the control in outer units and is approximately equal for cases 1 and 6, in which the same modes are removed at the same heights in outer units, but for different Reynolds numbers. These preliminary results suggest that the effect of the control does indeed scale in outer units. This could be expected, since the size of the self-similar structures we wish to control scales with their wall-normal distance. The premultiplied energy spectra for case 6, portrayed in figure 8, also become essentially identical to those of the uncontrolled case far enough above the target height, consistent with our previous findings at $Re_\tau = 550$. This further supports the idea that, far enough above the forcing region, turbulence exhibits outer-layer similarity, and the only change in the flow due to the control is the additional mean velocity ΔU^+ .

4. Conclusions

We have conducted a preliminary investigation into the effect of artificially removing certain length scales of the wall-normal velocity from the logarithmic region of turbulent channel flows, using direct numerical simulation. In this way, we control large-scale, logarithmic layer turbulent structures, whose size depends on their distance from the wall, without affecting the near-wall turbulent dynamics, essentially isolating their contribution to the drag from that of the other scales in the flow. The reduction in drag is observed as a positive, outward shift of the mean velocity profile above the height at which the length scales are removed. This can be explained by the balance of viscous and Reynolds shear stress in these controlled flows, compared to the uncontrolled reference case. In the vicinity of the forcing region, there is a small, but significant deficit in the Reynolds shear stress compared to the uncontrolled reference case, which results in a local increase in viscous stress. Therefore, dU/dy is locally larger than in the uncontrolled flow, resulting in a sudden relative increase in U . However, far enough above the forcing region, the viscous and Reynolds shear stress recover to uncontrolled values, as do the turbulent fluctuations. In this sense, the turbulence far from the wall is essentially unmodified except for this additional mean velocity, and eventually recovers outer-layer similarity. By comparing simulations at two friction Reynolds numbers, $Re_\tau = 550$ and 950, we verify, at least tentatively, that when the control is consistent in outer units, then its effect on the mean velocity is equivalent in outer units. This was to be expected since the structures we target scale with distance from the wall. While we have discussed the effect of removing certain length scales from the wall-normal velocity at various heights within the logarithmic region, it is still unclear what the optimal range of wavelengths to remove would be, and at which heights to remove them. This is an ongoing area of investigation in our research group.

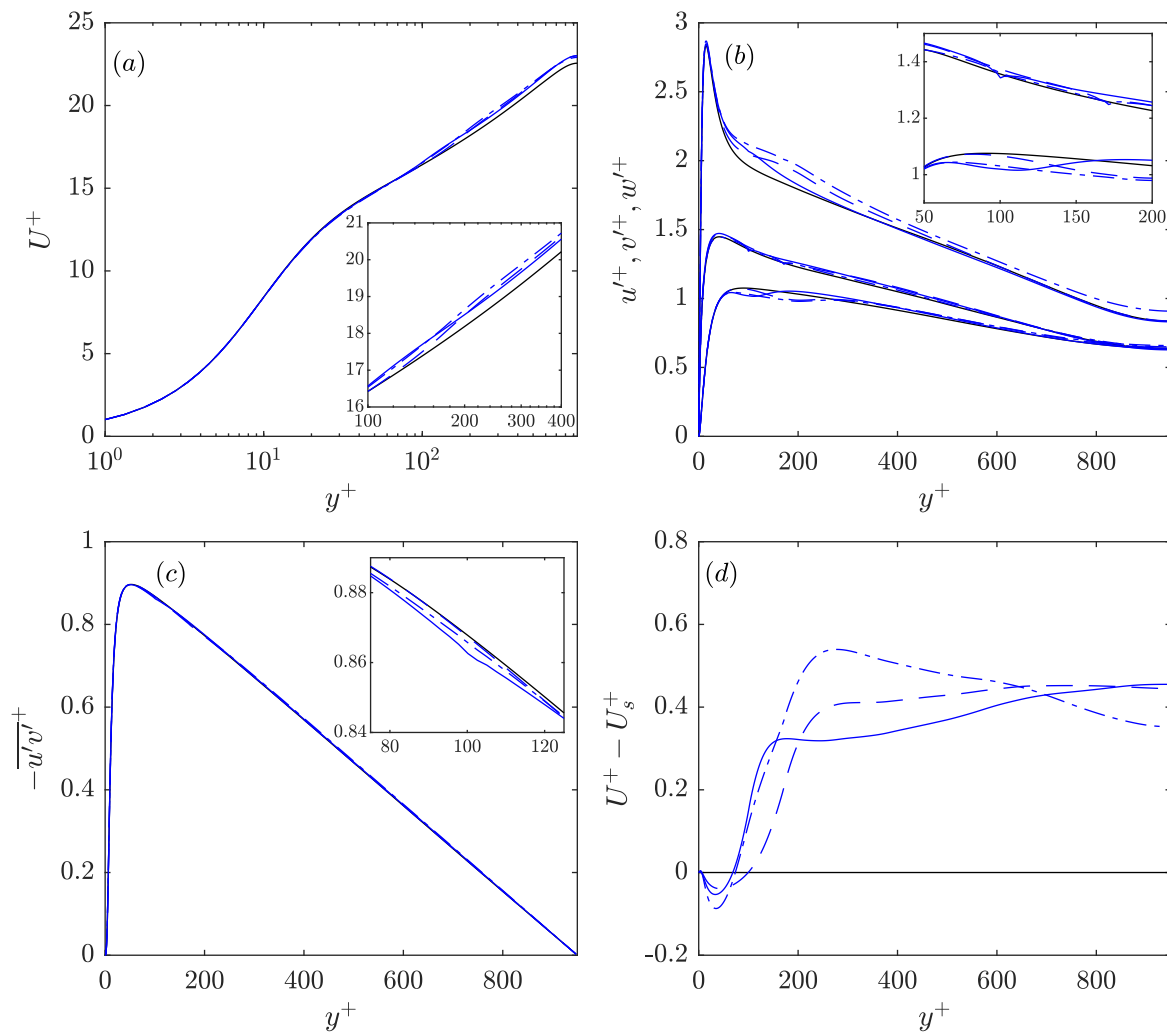


Figure 7. Statistics for cases at $Re_\tau = 950$, including $\Delta U^+(y^+) = U^+ - U_s^+$. Black lines, uncontrolled case; blue lines, controlled cases. See table 1 for line styles.

Acknowledgments

This work was funded in part by the European Research Council through the 2nd Coturb Madrid Summer Workshop. We also gratefully acknowledge the use of CSD3 under an EPSRC Tier-2 computing grant and SURFSara under a PRACE Tier-1 computing grant.

References

- [1] P. R. Spalart and J. D. McLean. Drag reduction: enticing turbulence, and then an industry. *Philos. Trans. Royal Soc. A*, 369:1556–1569, 2011.
- [2] P. Orlandi and J. Jiménez. On the generation of turbulent wall friction. *Phys. Fluids*, 6:634, 1994.
- [3] J. M. Hamilton, J. Kim, and F. Waleffe. Regeneration mechanisms of near-wall turbulence structures. *J. Fluid Mech.*, 287:317–348, 1995.
- [4] F. Waleffe. On a self-sustaining process in shear flows. *Phys. Fluids*, 9:883, 1997.
- [5] J. Jiménez and A. Pinelli. The autonomous cycle of near-wall turbulence. *J. Fluid Mech.*, 389:335–359, 1999.
- [6] R. García-Mayoral, G. Gómez-de-Segura, and C. T. Fairhall. The control of near-wall turbulence through surface texturing. *Fluid Dyn. Res.*, 51:011410, 2019.
- [7] F. H. Clauser. The turbulent boundary layer. *Adv. Appl. Mech.*, 4:1–51, 1956.

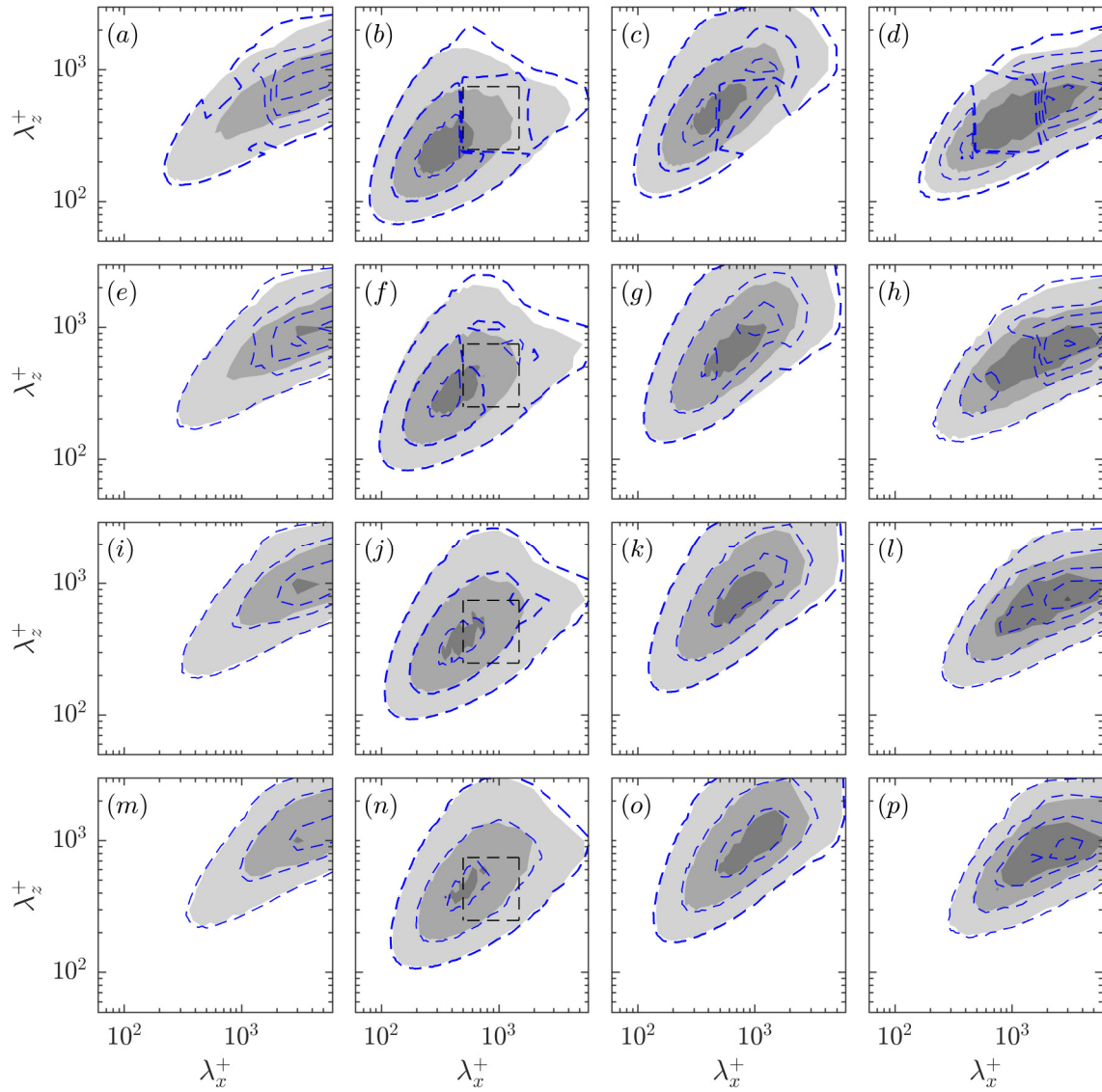


Figure 8. Premultiplied two-dimensional spectral densities of u^2 , v^2 , w^2 and uv for case 6 (blue dashed lines) compared to the uncontrolled case (filled contours) at (a–d) $y^+ = 173$, (e–h) $y^+ = 259$, (i–l) $y^+ = 350$, (m–p) $y^+ = 500$. The black dashed line encloses the wavelengths of v that are removed from the flow in the forcing region, y_f^+ .

- [8] H. Choi, P. Moin, and J. Kim. Active turbulence control for drag reduction in wall-bounded flows. *J. Fluid Mech.*, 262:75–110, 1994.
- [9] D. Gatti and M. Quadrio. Reynolds-number dependence of turbulent skin-friction drag reduction induced by spanwise forcing. *J. Fluid Mech.*, 802:553–582, 2016.
- [10] B. Nugroho, N. Hutchins, and J. P. Monty. Large-scale spanwise periodicity in a turbulent boundary layer induced by highly ordered and directional surface roughness. *Int. J. Heat Fluid Flow*, 41:90–102, 2013.
- [11] H. L. Bai, Kevin, N. Hutchins, and J. P. Monty. Turbulence modifications in a turbulent boundary layer over a rough wall with spanwise-alternating roughness strips. *Phys. Fluids*, 30:055105, 2018.
- [12] M. R. Abbassi, W. J. Baars, N. Hutchins, and I. Marusic. Skin-friction drag reduction in a high-Reynolds-number turbulent boundary layer via real-time control of large-scale structures. *Int. J. Heat Fluid Flow*, 67:30–41, 2017.
- [13] O. Flores and J. Jiménez. Hierarchy of minimal flow units in the logarithmic layer. *Phys. Fluids*, 22:071704, 2010.
- [14] J. Jiménez. Coherent structures in wall-bounded turbulence. *J. Fluid Mech.*, 842:P1, 2018.
- [15] J. A. Sillero, J. Jiménez, and R. D. Moser. One-point statistics for turbulent wall-bounded flows at Reynolds numbers up to $\delta^+ \approx 2000$. *Phys. Fluids*, 25:105102, 2013.
- [16] A. Guseva, M. P. Encinar, and J. Jiménez. Active flow control of the logarithmic layer. In *Proc. Div. Fluid Dyn.*, page B26.4. Am. Phys. Soc., 2019.
- [17] M. de Giovanetti, Y. Hwang, and H. Choi. Skin-friction generation by attached eddies in turbulent channel flow. *J. Fluid Mech.*, 808:511–538, 2016.
- [18] D. Chung, L. Chan, M. MacDonald, N. Hutchins, and A. Ooi. A fast direct numerical simulation method for characterising hydraulic roughness. *J. Fluid Mech.*, 773:418–431, 2015.
- [19] M. MacDonald, L. Chan, D. Chung, N. Hutchins, and A. A. Ooi. Turbulent flow over transitionally rough surfaces with varying roughness densities. *J. Fluid Mech.*, 804:130–161, 2016.
- [20] R. García-Mayoral and J. Jiménez. Hydrodynamic stability and breakdown of the viscous regime over riblets. *J. Fluid Mech.*, 678:317–347, 2011.
- [21] C. T. Fairhall and R. García-Mayoral. Spectral analysis of the slip-length model for turbulence over textured superhydrophobic surfaces. *Flow Turbul. Combust.*, 100:961–978, 2018.
- [22] J. Kim and P. Moin. Application of a fractional-step method to incompressible Navier–Stokes equations. *J. Comput. Phys.*, 59:308–323, 1985.
- [23] H. Le and P. Moin. An improvement of fractional-step methods for the incompressible Navier–Stokes equations. *J. Comput. Phys.*, 92:369–379, 1991.
- [24] A. Lozano-Durán and J. Jiménez. Effect of the computational domain on direct simulations of turbulent channels up to $Re_\tau = 4200$. *Phys. Fluids*, 26:011702, 2014.
- [25] A. A. Townsend. *The Structure of Turbulent Shear Flow*. Cambridge University Press, 1976.